PAPER

Current promoted micro-annealing in anodic TiO$_2$ tube arrays and its application in sensitized solar cells†

Yan Xiong,[a] Liang Tao,[b] Hong Liu*[ab] and Wenzhong Shen*[ab]

Crystallization in nanostructured materials is an important basis of solar cells and other nanoscience fields. For instance, crystalline TiO$_2$ for photovoltaic and photocatalysis applications is normally formed by high-temperature annealing above 450 °C for a long period of time (normally more than one hour). In this work, we have established a method to artificially induce crystallization in ordered anodic TiO$_2$ tube arrays at around room temperature for the first time. Assisted by the existence of an electric field in the reaction system, crystallization could take place at a much lower temperature than isothermal annealing. Aided by the low thermal conductivity of TiO$_2$, the sample surface temperature could be limited to an even lower value (below 130 °C). The as-fabricated samples could show significant efficiencies of up to 2.05% after being installed into back-side illuminated dye sensitized solar cells. Furthermore, a nearly monocrystalline-like structure could be formed through some simple physical and chemical manipulation. As a result, an efficiency of 3.51% could be achieved, together with V_{OC} = 0.63 V, J_{SC} = 13.03 mA cm^{-2}, and FF = 0.47. This method can easily realize high quality crystallization in nanostructures like TiO$_2$ tube arrays of a particular size. It can be helpful for the development of new solar cells and other opto-electronic devices, and hopefully for mechanistic studies of other materials as well.

1 Introduction

Crystallized semiconductor oxides such as TiO$_2$, ZnO and Cu$_2$O have demonstrated excellent characteristics for opto-electronics, new energy devices and other nanosciences. Among them, TiO$_2$ has attracted extremely intense attention due to its high thermostability,[1] flexibility for nanostructure formation,[2–4] tunable band structure,[5] photo catalytic properties[6] and lower cost compared to traditional semiconductors, aided by high internal quantum efficiencies,[7] large surface-to-volume ratios[8] and a tunable absorption range.[9,10] Among its wide applications, dye sensitized solar cells (DSSC) are among the most important. Since the first report on DSSCs by O'Regan and Grätzel in 1991,[8] they have attracted considerable interest as low-cost alternatives to silicon solar cells. A decade later, porous titania film and ordered TiO$_2$ nanotube (NT) arrays were reported,[11,12] having good dye absorption abilities and carrier conductivities. Recently, DSSCs on flexible substrates have also been developed which are suitable for mobile devices and easy to produce with roll-to-roll processes.[13]

Until now, the highest efficiency of a DSSC of 12.3% has been achieved using porous nanocrystalline TiO$_2$ as the photoanode and Co/ as the oxidation/reduction pair.[14] The efficiency of DSSCs based on nanotube arrays is still lower, possibly due to the trapping effect on electrons in the TiO$_2$ bulk by electrochemical oxidation.[15,16] However, compared to nanocrystalline porous films,[17–19] NT arrays are easier to control with uniform order, which means they are more flexible for multiple uses. In general, beside the sensitizer absorption and oxidation/reduction pair of the electrolyte, the carrier conductivity in the TiO$_2$ substrate (porous or as NT arrays) also plays an important role in DSSCs, no matter whether it is porous or based on NT arrays. Hence the crystallinity of the TiO$_2$ material becomes very important. As is commonly known, there are generally three kinds of structures of crystalline TiO$_2$: anatase, rutile and brookite, among which anatase has the best performance as a photoanode in DSSCs.[20,21]

To resolve this issue, it is important to obtain better crystallinity and a smaller boundary effect. Normal experimental methods consist of homogeneous conditions in thermal equilibrium, *e.g.*, sintering the sample in an oven at 450–550 °C, to achieve structures with good crystallinity and smaller boundary effects in TiO$_2$ photoanodes.[22,23] These kinds of conditions not only result in environmental problems and the increased complexity of fabrication procedures, but also create certain limits in the development of cell architectures, *e.g.*, for normal

[a]*Institute of Solar Energy, Department of Physics, Shanghai Jiao Tong University, 800 Dong Chuan Road, Shanghai 200240, People's Republic of China. E-mail: liuhong@sjtu.edu.cn; Fax: +86 21 54743243; Tel: +86 21 54743243*

[b]*Laboratory of Condensed Matter Spectroscopy and Opto-Electronic Physics, Key Laboratory of Artificial Structures and Quantum Control (Ministry of Education), Department of Physics, Shanghai Jiao Tong University, 800 Dong Chuan Road, Shanghai 200240, People's Republic of China. E-mail: wzshen@sjtu.edu.cn; Fax: +86 21 54747552; Tel: +86 21 54747552*

† Electronic supplementary information (ESI) available. See DOI: 10.1039/c2ta00810f

This journal is © The Royal Society of Chemistry 2013

J. Mater. Chem. A, 2013, **1**, 783–791 | **783**

high transparency flexible plastic substrates due to structural damage above 150 °C.[24,25] In recent research from different groups, crystallization phenomena at low ambient temperatures (less than room temperature) were discovered during electrochemical anodization.[26–29] We have found that the size and quantity of crystal grains in the anatase or rutile phase are increased by a greater temperature gradient over the TiO_2 film and named this effect "micro-annealing" due to its overall localized thermal behavior.[26] However, the crystallization in such a spontaneous process was so weak that it did not lead to a significant photovoltaic conversion efficiency in a solar cell. Moreover, the size of the tubes was limited to a small range since anodization and micro-annealing take place simultaneously at the same voltage. Due to those problems, the samples that underwent spontaneous micro-annealing showed no significant efficiencies after being installed in DSSCs. Furthermore, the so called current annealing method has been applied in metallurgy and some material processes by introducing an external current directly into the target material.[30–32] It introduces a certain kind of structural modification from normal thermal annealing, and has shown very good low temperature behavior. However, due to the high electronic resistivity and surface behavior of TiO_2, its application in TiO_2 nanotubes and solar cells remained a challenge.

In this work, we have investigated a novel experimental approach to obtain a crystalline TiO_2 tube array which can be directly applied in photovoltaic devices at low ambient temperatures. Current injection was carried out in the liquid phase with reversed polarity to avoid structural destruction by electrochemical reactions. Crystalline grains which generally had the anatase structure were formed at low temperatures, which are normally formed by thermal annealing in an oven at above 450 °C. In the meantime, though slowly increasing, the overall temperature of the sample was not higher than 130 °C during experiment. It exhibited a strong current annealing effect together with localized heat transfer, which was possibly aided by the high electronic resistivity and low thermal conductivity of TiO_2.[33–36] The as-fabricated TiO_2 resulted in improved efficiency after being installed into back-side illuminated DSSCs. With controlled thermostatic bath temperature, anodization voltage and subsequent chemical treatment, the crystallization was much enhanced. The sample has shown an improved efficiency of 3.51% after being directly installed into a back-side illuminated dye sensitized solar cell. Furthermore, unlike spontaneous micro-annealing in which the tube size is limited, crystallization using current injection can be performed for a controlled size of tubes. This novel method can shed light on the development of new thin film solar cells, and might stimulate the study of this nanomaterial in general.

2. Experimental

2.1 Fabrication of TiO_2 nanotube arrays

Ti sheets (0.25 mm thick, 99.7% purity, Sigma-Aldrich Co. Ltd, USA) were cleaned with methanol, ethyl alcohol, acetone and isopropyl alcohol in an ultrasonic bath in sequence prior to

the experiments. Highly ordered TiO_2 NTs were prepared by two-step anodization of the Ti sheet in a two-electrode cell (detail can be found in Fig. S1 in the ESI†). The first anodization was performed at 160 V at 5 °C for 60 min in ethylene glycol (with 0.18 M NH_4F and 1.0% H_2O). The second anodization was performed at 160 V/160 ± 5 V at 5 °C for 10 min in the same solution. The TiO_2 NT films used in following experiments have a standard inner and outer diameter of about 120 nm and 200 nm, respectively.

2.2 Current treatment and chemical modification of TiO_2 NTs

The current treatment was executed by reversing the polarity of the electrolysis pool with the original electrolyte for the two-step anodization of TiO_2 tubes. The reversed voltage was increased with a ramping speed of 1 V s^{-1}, and then kept constant at 300 V for 300 s. Then the TiO_2 film was carefully cleaned in deionized water in an ultrasonic bath. Chemical treatment with HF was applied between the two-step anodization and the current treatment. The TiO_2 film was firstly soaked in a 0.1% HF aqueous solution for 10 min at room temperature within airtight bottles and then cleaned with deionized H_2O. Digital pictures of TiO_2 NT films at different stages can be found in Fig. S2 in the ESI.†

2.3 Fabrication of DSSCs

After the chemical and current treatments, the TiO_2 NTs were immersed in 0.5 mM N719 dye (ruthenium 535-bisTBA) solution in ethanol for 12 h. The tested dye sensitized solar cells were back-side illuminated, using TiO_2 NT films based on Ti sheet as photoanodes and Pt covered glass as the counter electrode (platinum black, prepared by coating FTO glass with a 4 mM H_2PtCl_6 solution in ethanol and then heating in air at 200 °C for 60 min). The liquid electrolyte was injected into the cells by a syringe, and consisted of 0.1 M iodine (I_2), 0.1 M lithium iodide (LiI), 0.6 M tetra-butylammonium iodide and 0.5 M 4-tert-butyl pyridine in acetonitrile (CH_3CN, 99.9%).

2.4 Characterization of the materials and the solar cells

The surface morphologies of the samples were characterized by a field emission scanning electron microscope (FE-SEM, JEOL JSM). The elemental analysis was performed by energy dispersive X-ray (EDX) analysis during the FE-SEM observation. The detailed structural information of the TiO_2 NT materials was investigated by a transmission electron microscope (TEM, JEM-2100F, JEOL USA Inc.) and by selected area electron diffraction (SAED) during the HR-TEM measurements. The microstructures of the samples were also characterized by X-ray diffraction (XRD, D/max-2200/PC) with high intensity Cu Kα radiation ($\lambda = 1.5406$ Å). The photocurrent density–photovoltage (J–V) characteristics of the DSSCs with an effective area of 0.1 cm^2 were measured under AM 1.5 (100 mW cm^{-2}) illumination provided by a solar simulator (Oriel Sol 2A) with a Keithley 2400 source meter. Beside the data mentioned in the manuscript, the whole dataset can be found in Table S1 in the ESI.†

3 Results and discussion

3.1 Effect of current promoted micro-annealing

Ordered TiO_2 tubes were firstly fabricated by two-step anodic oxidation at a medium voltage (160 V) to produce ordered TiO_2 NTs of a suitable size.[37–39] To realize the micro-annealing artificially, the most applicable source of heat is direct current injection. However, direct current flow through the dry sample with the contact being the top-evaporated electrode led to no significant result since TiO_2 has a high electrical resistivity at around room temperature. The liquid electrical contact has significantly reduced the conductivity trouble caused by the TiO_2 due to its large contact area with the electrolyte. In this work, the as-fabricated TiO_2 tube arrays were treated with a voltage of 300 V in the original electrolysis pool for 300 s (plus 300 s ramping period). In order to avoid the side effects caused by continued anodization and dissolution in this process, the polarity of the voltage was reversed. The samples were then morphologically and structurally studied by scanning electron microscopy (SEM), high resolution transmission electron microscopy (HR-TEM), selected area electron diffraction (SAED) and X-ray diffraction (XRD), as shown in Fig. 1 and 2.

Before the current treatment, the NTs have an average length of ~20 μm and diameter of ~120 nm, as shown in Fig. 1(a) and (b). Meanwhile, the HR-TEM and SAED images in Fig. 1(c) and (d) show that the as-fabricated tubes were amorphous. After current injection at an ambient temperature of −5 °C, as shown in Fig. 1(c′) and (d′), certain crystalline structures had formed in the tubes. The characteristic distance of those structures was $a = 0.375$ nm, which is comparable with the lattice constant $a = 0.378$ nm of the anatase structure.[26,40,41] Further evidence can be found in Fig. 2 which shows XRD measurements. The peaks in the range 24.0–25.5° should belong to the (101) surface of the anatase phase and structures close to the anatase phase.[42] The diverse shifts should be due to different lattice spacings in the (101) direction (in most cases longer than the standard anatase phase)[43] which were possibly induced by inhomogeneous heat distribution from the annealing current. The peak at 47.5°
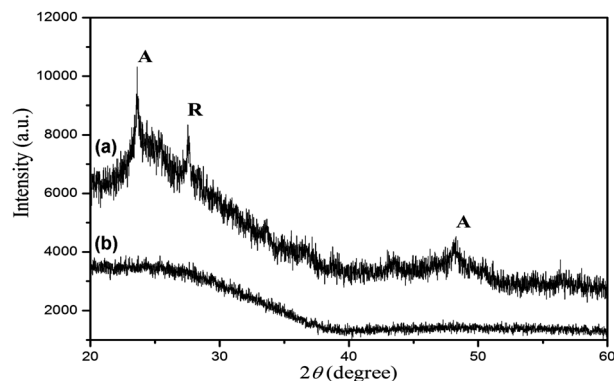

Fig. 2 XRD pattern of TiO_2 NTs: (a) after current annealing at −5 °C; (b) after two step anodization. A: anatase, R: rutile.

corresponds to the (200) crystal surface of the anatase phase. The peak at 27.5° is the (110) crystal surface, which belongs to the rutile phase.[41,44] These facts indicate the formation of certain anatase-like and rutile-like crystalline grains inside the current treated samples. In the meantime, the macroscopic temperature increase inside the sample chamber did not exceed 130 °C (the detailed data can be found in Fig. S3 in the ESI†). Additionally, it can also be seen that some peaks of the standard anatase or rutile diffraction patterns were missing in the XRD shown in Fig. 2, which indicates some kind of anisotropic effect of this crystallization process, though the SAED pattern still shows a nanocrystalline phase. One possible origin of this anisotropy might be the anisotropic heat generation by the current flow under the influence of the tube morphology.

Due to the involvement of artificially applied current and the localized heat effect in the crystallization process, this phenomenon was thus named current promoted micro-annealing (which can be abbreviated to CPMA). Compared to spontaneous micro-annealing (can be abbreviated to SMA) at a constant voltage of 210 V over a long time period (3600 s), the voltage during the tube growth was relatively low (160 V), and that in the subsequent current treatment was higher (300 V) and over a much shorter time period (300 s ramping + 300 s constant).[26,29,45] It should also be noted in Fig. 1(a′) that some kind of sediment was formed at the top surface of the tube arrays after the current treatment, which might negatively influence the carrier transport and also decrease the effective absorption of the sensitizers in the tube arrays. This roughness might have been contributed to by chemical etching by redistributed F^- anions and the precipitation of TiF_6^{2-} anions both flowing from the inside of the tubes driven by electrical forces.

3.2 CPMA under different temperatures and its performance in dye sensitized solar cells

As shown in the previous section, the crystallization of TiO_2 inside the initially amorphous TiO_2 tubes can occur with a direct reversed current applied to the TiO_2 tube arrays over a short time period at a low ambient temperature. It is therefore important to investigate the key factors in this process to enable the possibility of manipulating it. In the SMA process, the
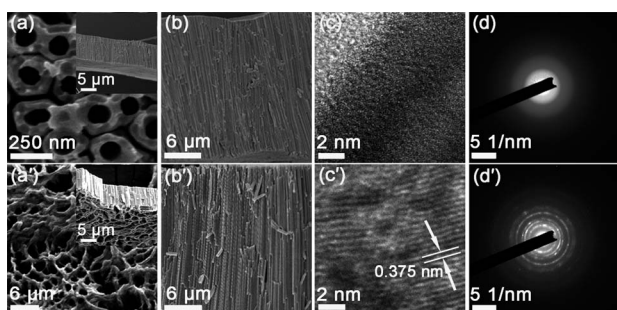

Fig. 1 Morphological and structural studies of TiO_2 NTs at different stages: (a) and (a′) top view of as-prepared TiO_2 NTs before and after current treatment, respectively; the insets give an overview on a larger scale; (b) and (b′) lateral view of TiO_2 NTs before and after current annealing at −5 °C, respectively; (c) and (c′) HR-TEM images of as-prepared TiO_2 NTs before and after current treatment, respectively; (d) and (d′) SAED of the TiO_2 NTs before and after current annealing at −5 °C, respectively.

This journal is © The Royal Society of Chemistry 2013

J. Mater. Chem. A, 2013, **1**, 783–791 | **785**

temperature gradient over the TiO_2 sheet (from the inside of the sample chamber to the outer electrolyte) is an important factor.[26] To test its relevance in CPMA, the temperature gradient could be increased either by lowering the ambient temperature controlled by the thermal bath or raising the temperature in the sample chamber using a heat source implanted inside the chamber. According to the real experimental conditions, the former method was more applicable. Therefore these experiments with CPMA were generally carried out by varying the ambient temperature to investigate the temperature effect.

The results are illustrated by the structural study of samples under different ambient temperatures in Fig. 3. It can be observed that TiO_2 treated at an ambient temperature of 5 °C was still amorphous-like, as shown in Fig. 3(a) and (b). On the contrary, when TiO_2 tubes were treated at a lower temperature of −10 °C, the crystallization became more significant than at −5 °C, as shown in Fig. 3(a′) and (b′). This result clearly supported the assertion that a larger temperature gradient can enhance the whole crystallization process. Moreover, more XRD peaks appeared at lower ambient temperature as shown in Fig. 3(c). The peak at about 54.2° (related to the anatase (211) direction) was enhanced compared to that in Fig. 2.[41] This has further proved the enhancement of the crystallization by a greater temperature gradient.

Subsequently, the films consisting of TiO_2 tube arrays fabricated at different temperatures were installed into backside illuminated dye sensitized solar cells (with N719 dye as the sensitizer). As shown in Fig. 3(d), the solar cells containing TiO_2 tubes fabricated at −5 °C and −10 °C had efficiencies of 1.34% and 2.05%, respectively. The TiO_2 film processed at −10 °C with a higher efficiency had an open circuit voltage (V_{OC}) of 0.52 V, a short circuit current density (J_{SC}) of 11.24 mA cm^{-2}, and a fill factor (FF) of 0.36. The higher efficiency at lower treatment temperature is in a large part due to the better crystallinity of the TiO_2 photoanode. Furthermore, as commonly known in solar cell measurements, the absolute values of the slopes near the short circuit current (k_{SH}) the open circuit voltage (k_S)

correspond reciprocally to the shunt and series resistance of the cell, respectively. From the J–V curves shown in Fig. 3(d) k_{SH} and k_S of the sample annealed at −10 °C were calculated to be $1.28 \times 10^{-2} \ \Omega^{-1} \ cm^{-2}$ and $2.80 \times 10^{-2} \ \Omega^{-1} \ cm^{-2}$, respectively, both higher than the corresponding values of $6.29 \times 10^{-3} \ \Omega^{-1} \ cm^{-2}$ and $2.48 \times 10^{-2} \ \Omega^{-1} \ cm^{-2}$ at −5 °C, which indicated that both the cell series and shunt resistances were lower at lower temperature with higher efficiency. The lower series resistance was apparently due to better carrier conductance in the better crystallized TiO_2 photoanode, which is advantageous for the fill factor and the real output of the cell. However, the lower shunt resistance could reduce the fill factor and output of the cell, which is possibly related to lateral contacts due to roughness of the tube surface whose conductance was improved by the better crystallization. Despite the resistance problem, −10 °C still emerged as the best condition due to the significant increase in efficiency and therefore was the basic condition used for the manipulation experiments. Yet there are still possibilities for making further improvements by certain chemical or physical treatments.

3.3 CPMA processed TiO_2 tubes under chemical treatment

Previous sections have discussed the current stimulated micro-annealing effect and its application in DSSCs, as well as some disadvantages. To resolve the existing problems, some chemical treatment could be applied, e.g., a certain amount of HF was helpful to increase the effective area of TiO_2 tube arrays due to the formation of secondary structures, according to previous work from our and other groups.[42,46,47] It was also expected that a high concentration of F$^-$ anions could influence the morphological properties at the TiO_2 surface. So HF will hopefully reduce the problems described in the previous sections and improve the as-fabricated DSSCs. To assess this, HF of different concentrations was applied on the TiO_2 sample after anodization and before the inverse current injection. As an example, the morphological and structural studies of the sample treated with 0.1% HF are shown in Fig. 4. First, as shown in Fig. 4, after being immersed in HF for 10 min and before the current injection, the tube surface was etched slightly
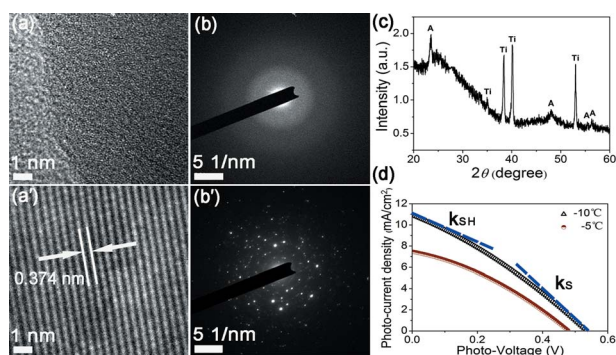

Fig. 3 Analysis of the TiO_2 NTs fabricated under different ambient temperatures and the performances of the cells assembled with them: (a) and (a′) HR-TEM of TiO_2 NTs after current annealing at 5 °C and −10 °C, respectively; (b) and (b′) SAED of TiO_2 NTs after current annealing at 5 °C and −10 °C, respectively; (c) XRD pattern of the sample after current annealing at −10 °C; (d) J–V characteristics of the DSSCs made from TiO_2 NTs annealed at −5 °C and −10 °C. k_{SH} and k_S are the absolute values of the slopes of the J–V curves near J_{SC} and V_{OC}, respectively.
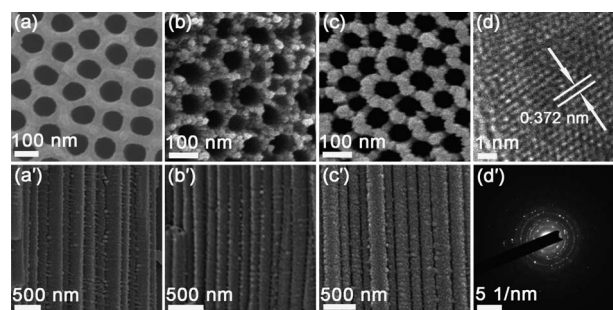

Fig. 4 Morphological and structural studies of TiO_2 NTs with HF treatment at different stages: (a) and (a′) top and lateral view of TiO_2 NTs after two-step anodization; (b) and (b′) top and lateral view of TiO_2 NTs with 0.1% HF treatment; (c) and (c′) top and lateral view of TiO_2 NTs with 0.1% HF treatment after current annealing; (d) and (d′) HR-TEM and SAED images of the TiO_2 NTs with 0.1% HF treatment after current annealing.

786 | J. Mater. Chem. A, 2013, 1, 783–791

This journal is © The Royal Society of Chemistry 2013

compared to the initial sample. Second, after the current injection, the irregular morphological change at the top surface of the tube arrays shown in Fig. 1(c) disappeared when the sample was treated by current injection with HF, as illustrated by Fig. 4(c) and (c′). In the meantime, certain island-shaped secondary structures developed at the surface of the tubes. The HR-TEM and SAED images in Fig. 4 show that the microstructure of the TiO$_2$ with HF treatment remained well organized compared to that treated by current injection without HF treatment.

These behaviors were quite similar to those for samples treated by HF at other concentrations in the experimental range (0–0.35%). To further investigate the changes under these different conditions, the performances of these samples needed to be characterized after being installed into solar cells. The *J–V* curves of the as-fabricated DSSCs are shown in Fig. 5. From 0 to 0.1% HF, the cell efficiency increased with increasing HF concentration and from 0.1% to 0.35% HF, the cell efficiency decreased. Apparently, the cell achieved its highest efficiency of 2.74% at 0.1% HF concentration, with $V_{OC} = 0.56$ V, $J_{SC} = 15.96$ mA cm^{-2}, and FF = 0.34. Compared to the efficiency of 2.05% for the sample without any HF treatment, it was a significant improvement. This improvement can be at least partly attributed to more effective dye absorption due to the removal of the top surface sediment shown in Fig. 1(a′).

Furthermore, slope measurements of the *J–V* curves have exposed more complicated facts behind the change in efficiency. From 0 to 0.1% HF, k_S increased from 2.80×10^{-2} Ω^{-1} cm^{-2} to 3.63×10^{-2} Ω^{-1} cm^{-2}, while k_{SH} increased from 1.28×10^{-2} Ω^{-1} cm^{-2} to 1.84×10^{-2} Ω^{-1} cm^{-2}, which meant both the series and shunt resistance decreased with increasing HF concentration. The decrease in the series resistance can be attributed to the removal of the top covering. Despite that, the shunt resistance was also reduced, which was negative. From 0.1% to 0.35% HF, k_S decreased from 3.63×10^{-2} Ω^{-1} cm^{-2} to 2.08×10^{-2} Ω^{-1} cm^{-2}, while the k_{SH} decreased from 1.84×10^{-2} Ω^{-1} cm^{-2} to 2.69×10^{-3} Ω^{-1} cm^{-2}. This indicates that

both series and shunt resistance increased with increasing HF concentration. In this range of conditions, a high concentration of HF was helpful to increase the shunt resistance, however, the series resistance was also increased and the efficiency was lower. Apparently, such effects can both be induced by the structural destruction by the etching effect of F$^-$ anions on the tubes. Overall, although the samples treated at 0.1% HF had the highest efficiencies, they didn't have the highest shunt resistances, which meant their fill factors and real outputs were still not optimized. Considering the results in this and previous sections, it will be necessary to find a way to improve the cell efficiency without significant sacrifice of the fill factor, for example, improving the structural ordering and the morphological homogeneity.

3.4 CPMA treated TiO$_2$ tube arrays with modulated anodic voltage and HF

Previous results have demonstrated that DSSCs fabricated with crystallized TiO$_2$ NT arrays treated by a reversed current show significantly efficiencies, and can be improved by chemical treatment with HF prior to the inverse current injection. It has also been found that chemical treatment was not enough to optimize the fill factor due its possible damage of the bulk of the tubes at high concentrations and the limited increase of the shunt resistance. Fortunately, it has been discovered in our previous work that the morphology of the TiO$_2$ NTs can be adjusted by controlling the mechanical stirring rate or the rapidly periodically modulated anodic voltage.[48] Combining this finding with the CPMA and HF treatment, it is expected that better ordered, straight and compact TiO$_2$ NTs with secondary fine structures will be obtained so that the negative influence of the chemical treatment might be reduced and the shunt resistance increased without sacrificing the efficiency.

To ensure better identity of this study, all the following experiments were preliminarily carried out with an HF concentration of 0.1% based on the result from the previous section. As demonstrated in Fig. 6(a) and (a′), the as-fabricated tube arrays with an oscillating voltage (160 ± 5 V) were well
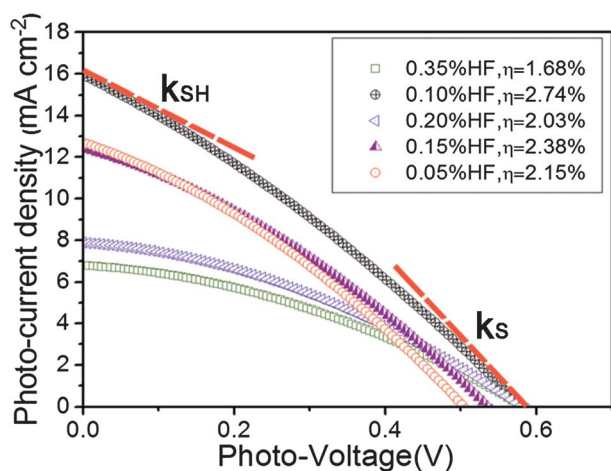

Fig. 5 *J–V* characteristics of dye-sensitized solar cells (using N719) with TiO$_2$ NTs treated by HF aqueous solutions of various concentrations, at a constant illumination of 100 mW cm^{-2}.
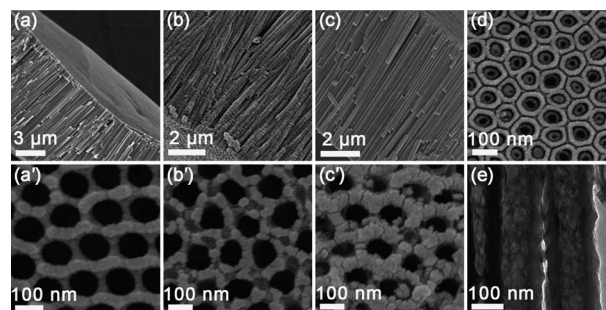

Fig. 6 Morphological and structural studies of TiO$_2$ NTs at different stages: (a) and (a′) lateral and top view of TiO$_2$ NTs with modulated voltage (160 ± 5 V); (b) and (b′) lateral and top view of TiO$_2$ NTs with modulated voltage after 0.1% HF treatment; (c) and (c′) lateral and top view of TiO$_2$ NTs with modulated voltage and 0.1% HF treatment after annealing at −10 °C; (d) back view of the TiO$_2$ NTs and (e) the TEM image of the TiO$_2$ NTs after current annealing with modulated voltage and HF treatment.

This journal is © The Royal Society of Chemistry 2013

J. Mater. Chem. A, 2013, **1**, 783–791 | **787**

ordered and had good surface quality. After HF treatment and before the current injection, the tubes shown in Fig. 6(b) and (b′) show a similar change to the samples with only HF at this stage. Finally, as shown in Fig. 6(c) and (c′), the tubes after current injection were apparently quite straight and ordered, containing more significant and homogeneously distributed secondary structures at the surface compared to the result with only HF treatment (shown in Fig. 4). The TEM image in Fig. 6(e) demonstrates the inner morphology of the TiO_2 NTs after current annealing, showing that the secondary structures were also formed at the insides of tube walls.

Furthermore, structural studies by HR-TEM, SAED and XRD showed good crystallinity of the TiO_2 tubes anodized by a modulated voltage after HF and current annealing, which can be observed in Fig. 7. The crystallinity was more ordered so that even a monocrystalline-like phase could be detected from the SAED pattern in Fig. 7(a′). Furthermore, as is shown by the XRD study in Fig. 7(b), the anatase (101) peak at 25.4° and the (211) peak at 54.2° were significantly enhanced, which suggested that the crystallization was improved over a large range of the sample and not localized in certain areas. Consequently, these samples showed significantly improved performances after being mounted into back side illuminated DSSCs, as shown by the J–V characteristics in Fig. 8 in comparison with previous results obtained by high temperature annealing under similar conditions. A final efficiency of 3.51% could be achieved, with $V_{OC} = 0.63$ V, $J_{SC} = 13.03$ mA cm^{-2}, and FF = 0.47. The efficiency is about 28.10% higher than for the CPMA treated sample with only HF chemical treatment and 56.0% higher than the sample annealed at high temperature (500 °C) as normal under a similar anodization voltage (also shown in Fig. 8). This result shows that CPMA can achieve quite a significant efficiency even when compared to the normal experimental method.

Moreover, the absolute values of the slopes near the open circuit voltage and short circuit current have shown significant improvement to a greater extent than the efficiency, as can be seen from Fig. 8. For the sample optimized with an oscillating voltage and 0.1% HF, on the one hand, k_S was 3.83×10^{-2} Ω^{-1} cm^{-2}, higher than the value of 3.6×10^{-2} Ω^{-1} cm^{-2} for the sample with only HF, which corresponded to a lower series
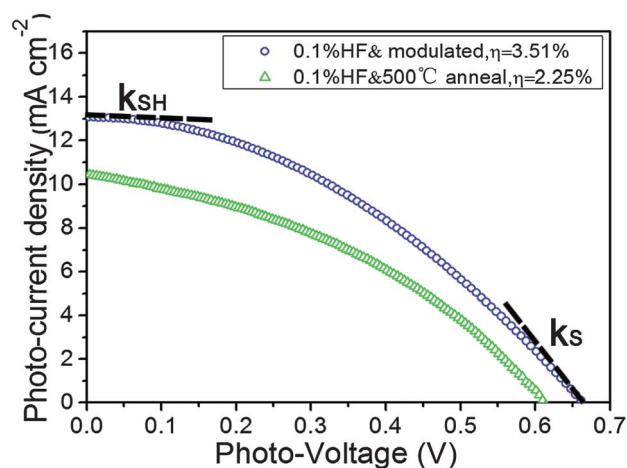

Fig. 8 J–V characteristics of dye-sensitized solar cells (using N719) with TiO_2 NTs treated by current injection with 0.1% HF and a modulated voltage (160 ± 5 V), and with 0.1% HF treatment without a modulated voltage and with 500 °C annealing with a modulated voltage, at a constant illumination of 100 mW cm^{-2}.

resistance. On the other hand, k_{SH} was 1.07×10^{-3} Ω^{-1} cm^{-2}, much smaller than the value of 1.84×10^{-2} Ω^{-1} cm^{-2} for the sample only treated by HF, indicating a much increased shunt resistance. As a result, the fill factor was significantly increased over that for the sample with only chemical treatment, and the efficiency was better. This has proved that a significant improvement in both the efficiency and fill factor can be simultaneously achieved by the combination of simple physical and chemical manipulations.

3.5 Related discussions on the formation and manipulation of CPMA

The CPMA using a high reversed current at a low ambient temperature has been demonstrated in the above sections. Significant crystallization can be achieved through this experimental method and can be enhanced by lowering the ambient temperature. To get better indication of the mechanism of this process, it can be helpful to consider current annealing which is normally applied in metallurgy and the previously reported spontaneous micro-annealing (SMA).[26,30–32] In current annealing, the application of current significantly encourages crystallization to take place, in comparison with normal isothermal annealing.[30] In the SMA process, the heat comes from both the current flow and the oxidation reaction,[49,50] and the grains form during the growth of oxide, which enhances the heat localization, but somehow limits the further development of the crystallization process.[26]

Due to the limit of the current advance in mechanistic investigations so far, some details of these processes are still not totally understood. However with the current knowledge, a possible general description of CPMA can be sketched out as follows: first, the heat was mainly generated by the strong current at the oxide layer due to its high electrical resistance, which offered energy for the atoms to overcome the activation energy for crystallization. At the same time, compared to thermal annealing, the current provided a noticeable reduction
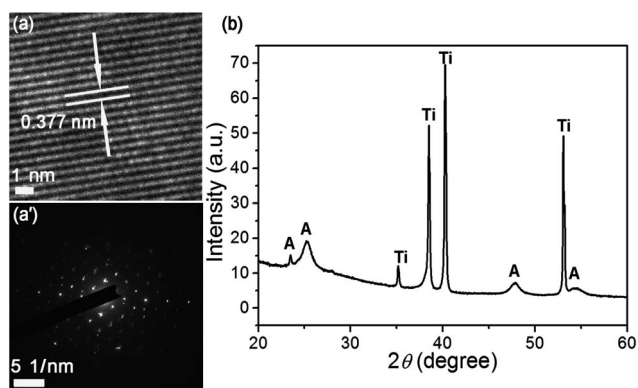

Fig. 7 Morphological and structural studies of CPMA treated TiO_2 NTs preliminarily anodized by a modulated voltage (160 ± 5 V) at −10 °C, with 0.1% HF: (a) and (a′) HR-TEM and SAED; (b) XRD pattern.

788 | J. Mater. Chem. A, 2013, **1**, 783–791

This journal is © The Royal Society of Chemistry 2013

in the thermal budget and a decrease of the exponent of crystallization.[30] Therefore the temperature which is necessary for crystallization will be significantly lower than the normal value for thermal annealing. Second, due to the low heat conductance of the TiO_2 (3 W m^{-1} K^{-1} at -10 °C, 3.5 W m^{-1} K^{-1} at RT and 3.75 W m^{-1} K^{-1} at 130 °C),[34] the Ohmic heat was localized to some degree so that the temperature at the probed position (where TiO_2 contacted the Ti substrate) remained even lower ($T_{max} < 130$ °C). Finally, the activated TiO_2 became crystallized and released energy at the low temperature side (where TiO_2 contacted the electrolyte), as happened in the SMA process.[26] If the ambient temperature is lower, such a relaxation process is then enhanced and so is the annealing process.

Moreover, the electronic and heat resistance is higher in amorphous TiO_2 than in anatase or rutile,[51] therefore more heat can be generated in the amorphous part between the crystal grains, which enhanced the crystallization at these positions.[30] In SMA, the crystallization was rapidly terminated when the nanocrystals moved away from the heat source at the bottom of the tube due to the tube growth.[26] Consequently, crystallization in CPMA can take place over larger time and space scales than in SMA, and a much stronger crystallization effect is induced. By suitably adjusting the ambient temperature, a nearly monocrystalline-like structure could be formed. It was also partly contributed to by the stronger current flow in CPMA under a higher voltage of 300 V, compared to the voltage of 210 V during spontaneous micro-annealing (data can be found in Fig. S4 in the ESI†). Finally, in SMA, the anodization and crystallization take place at the same voltage, so the size of the tubes is limited to a small range. But in CPMA, localized crystallization could result in the formation of different sizes of tubes, taking a much shorter treatment time. Therefore current injection is generally quite an efficient method which can be easily applied not only to TiO_2 treatment, but also to other similar materials.

Nevertheless, compared to the annealing process at a high ambient temperature (>450 °C) in the oven, CPMA can also induce some negative effects in the application of TiO_2 NTs in DSSCs, *i.e.*, some morphologically very disordered surface coverings were formed after treatment by a high current for a short time, as shown in Fig. 1. This effect was likely to be related to the dissolution and re-precipitation of TiO_2 near the top surface of the tube arrays, although the whole sample was negatively polarized during current annealing. Compared to the mechanism studies from previous works, this effect was possibly contributed to by the redistribution of F$^-$ anions that flow from the electrolyte that originally filled the tubes to the area near the top surface driven by the electrical force of the applied voltage.[26,48] Fortunately, this negative effect was compensated for by the addition of HF, which was widely applied for different purposes in the nanostructure fabrication. As is commonly known, a typical reaction occurring during TiO_2 tube formation is as below, which can be reversible under some conditions:[42]

$$TiO_2(s) + 4H^+ + 6F^- \leftrightarrow TiF_6^{2-} + 2H_2O \qquad (1)$$

During the study of TiO_2 NTs, this chemical can be used as a surface modifier to produce secondary structures in order to increase the effective surface for DSSCs.[42,46,52] In this work, it was found that HF diminished the very disordered layer on the top surface after current annealing, as shown in Fig. 1 and 4. This might be related to another difference between this experiment and the normal high temperature annealing: as shown in the EDX spectra in Fig. 9, F$^-$ anions still existed after annealing, instead of leaving the reaction system due to high temperatures of over 450 °C. Therefore, the simplest explanation for this is the inhibition of the re-precipitation of TiO_2 at the top surface of the TiO_2 tube arrays under a high F$^-$ concentration during current annealing, according to previous related work.[42]

Though the addition of HF can remove the porous layer and increase the shunt resistance, it can also lead to a negative effect on the series resistance, as has been shown in previous sections. According to the previous work,[42] such an influence by HF treatment is due to structural damage on the tubes due to chemical etching by F$^-$ anions, which decreases the electronic conductivity of the tube arrays and increase the series resistance of the solar cell. In this experiment, although the sample was negatively polarized during the current annealing, the temperature near the sample surface was also increased compared to normal conditions, which accelerated the chemical etching process. When the preliminary periodically modulated voltage was applied, significantly smoother and better ordered tube arrays were produced due to the reaction–diffusion processes of some species (TiO_2, TiF_6^{2-}, F$^-$, O^{2-}) under the influence of the periodic electric field.[44] As commonly known for corrosion processes, chemical etching is enhanced when the surface is more irregular.[53] Therefore a plausible consequence is that less structural damage can be induced by HF treatment at the tube surfaces, which can lead to significant improvement for the performance of as-fabricated DSSCs.[42] It is also plausible to consider that with less structural damage on the tube surfaces, a more homogeneous current flow can be induced, therefore the crystallization induced by current annealing can be improved.

Finally, it will naturally be a risk in current annealing to apply an inverse applied pool potential with copper as the counter electrode in a two-electrode system due to subsequent Cu contamination of the TiO_2 material by the anodization of
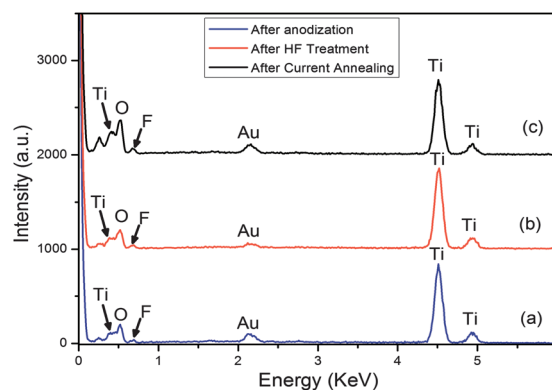

Fig. 9 EDX spectroscopy of the TiO_2 NTs at different stages: (a) after anodization; (b) after HF treatment; (c) after current annealing.
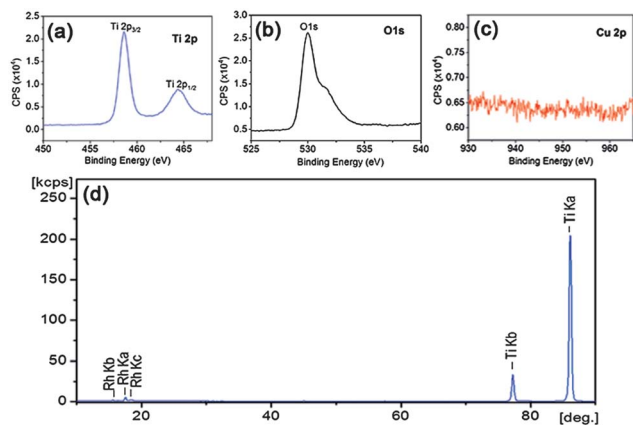
Fig. 10 Elemental analysis of the as-fabricated TiO$_2$: (a)–(c) XPS spectra of Ti, O and Cu; (d) XRF spectrum.

copper. It has been found by inductively coupled plasma (ICP) measurements that the concentration of the Cu component in the electrolyte exhibited a slight increase of 0.75 to 1.95 ppm after current treatment. However, no Cu contamination was detected in the as-fabricated TiO$_2$ sample by elemental analysis methods such as EDX shown in Fig. 9, X-ray photoemission spectroscopy (XPS) or X-ray fluorescence (XRF) shown in Fig. 10 (with sensitivity at the ppm level). Since the sample surface was subsequently cleaned by stirred deionized water after current treatment and before installation into a solar cell, the possible dominant influence of Cu is its doping into the TiO$_2$ bulk during the current treatment. Considering the results of the above measurements, the low diffusivity of Cu in the solid,[54] the short treatment time and the relatively low sample temperature, the possible Cu contamination of TiO$_2$ can be excluded in this work. Additionally, due to the semiconducting nature of TiO$_2$, the possible effect of the polarity shift on the absolute value of the current has also been measured (can be found in Fig. S5 in the ESI†). It was found that the polarity shift had no big influence on the absolute value of the current (in fact, the current with an inverse potential was a bit higher). Therefore the thermal effect of the current annealing was not negatively influenced by the inverse current injection.

4 Conclusion

To summarize this work, the following three points can be concluded here: (1) by reversed current annealing in a short period of time, anodic TiO$_2$ nanotube arrays can be effectively crystallized and show significant conversion efficiency after being assembled into sensitized solar cells; (2) crystallization in the TiO$_2$ nanotubes can be enhanced resulting in nearly crystalline structures by changing the ambient temperature and thus the efficiencies of as-fabricated solar cells are improved; (3) chemical and physical treatment by HF and an oscillating voltage can counteract the negative morphological change brought about by current annealing and further improve the crystallization and the cell performance. Generally, this phenomenon offers an effective method to fabricate a

nanostructured TiO$_2$ substrate without a high temperature process, therefore it will hopefully expand the application of this material or similar materials to wider conditions, for example, on fragile or flexible substrates. Finally, studies on the localization effect of heat might be considerably helpful for the investigation of structural formation in other electrochemical and thermochemical reaction systems.

Acknowledgements

Notes and references

1 Y.-H. Tseng, H.-Y. Lin, C.-S. Kuo, Y.-Y. Li and C.-P. Huang, *React. Kinet. Catal. Lett.*, 2006, **89**, 63–69.
2 C. A. Grimes and G. K. Mor, *J. Phys. Chem. C*, 2009, **113**, 7996–7999.
3 J. Lin, K. Liu and X. Chen, *Small*, 2011, **7**, 1784–1789.
4 B. Liu and E. S. Aydil, *J. Am. Chem. Soc.*, 2009, **131**, 3985–3990.
5 N. Serpone, *J. Phys. Chem. B*, 2006, **110**, 24287–24293.
6 Y. Kondo, H. Yoshikawa, K. Awaga, M. Murayama, T. Mori, K. Sunada, S. Bandow and S. Iijima, *Langmuir*, 2007, **24**, 547–550.
7 J. B. Sambur, T. Novet and B. A. Parkinson, *Science*, 2010, **330**, 63–66.
8 B. O'Regan and M. Grätzel, *Nature*, 1991, **353**, 737.
9 P. V. Kamat, *J. Phys. Chem. C*, 2008, **112**, 18737–18753.
10 A. Kongkanand, K. Tvrdy, K. Takechi, M. Kuno and P. V. Kamat, *J. Am. Chem. Soc.*, 2008, **130**, 4007–4015.
11 C. A. G. Dawei Gong, O. K. Varghese, W. Hu, R. S. Singh, Z. Chen and E. C. Dickey, *J. Mater. Res.*, 2001, **16**, 3331–3334.
12 V. Zwilling, M. Aucouturier and E. Darque-Ceretti, *Electrochim. Acta*, 1999, **45**, 921–929.
13 I. Masashi and M. Tsutomu, *Jpn. J. Opt.*, 2006, **35**(11), 564–569.
14 A. Yella, H.-W. Lee, H. N. Tsao, C. Yi, A. K. Chandiran, M. K. Nazeeruddin, E. W.-G. Diau, C.-Y. Yeh, S. M. Zakeeruddin and M. Grätzel, *Science*, 2011, **334**, 629–634.
15 C. He, Z. Zheng, H. Tang, L. Zhao and F. Lu, *J. Phys. Chem. C*, 2009, **113**, 10322–10325.
16 L. M. Peter, *Phys. Chem. Chem. Phys.*, 2007, **9**, 2630–2642.
17 T. R. B. Foong, Y. Shen, X. Hu and A. Sellinger, *Adv. Funct. Mater.*, 2010, **20**, 1390–1396.
18 Z. R. Tian, J. A. Voigt, J. Liu, B. McKenzie and H. Xu, *J. Am. Chem. Soc.*, 2003, **125**, 12384–12385.
19 D. Wang, F. Zhou, Y. Liu and W. Liu, *Mater. Lett.*, 2008, **62**, 1819–1822.
20 D. Cahen, G. Hodes, M. Grätzel, J. F. Guillemoles and I. Riess, *J. Phys. Chem. B*, 2000, **104**, 2053–2059.
21 N. G. Park, J. van de Lagemaat and A. J. Frank, *J. Phys. Chem. B*, 2000, **104**, 8989–8994.

22 C.-J. Lin, W.-Y. Yu and S.-H. Chien, *J. Mater. Chem.*, 2010, **20**, 1073–1077.

23 Q. Zheng, H. Kang, J. Yun, J. Lee, J. H. Park and S. Baik, *ACS Nano*, 2011, **5**, 5088–5093.

24 L. Grinis, S. Kotlyar, S. Rühle, J. Grinblat and A. Zaban, *Adv. Funct. Mater.*, 2010, **20**, 282–288.

25 Y. Kijitori, M. Ikegami and T. Miyasaka, *Chem. Lett.*, 2007, **36**, 190–191.

26 H. Liu, L. Tao and W. Z. Shen, *Electrochim. Acta*, 2011, **56**, 3905–3913.

27 S. P. Albu, A. Ghicov, S. Aldabergenova, P. Drechsel, D. LeClere, G. E. Thompson, J. M. Macak and P. Schmuki, *Adv. Mater.*, 2008, **20**, 4135–4139.

28 S. K. Poznyak, D. V. Talapin and A. I. Kulak, *J. Electroanal. Chem.*, 2005, **579**, 299–310.

29 S. Yoriya, G. K. Mor, S. Sharma and C. A. Grimes, *J. Mater. Chem.*, 2008, **18**, 3332–3336.

30 A. Rogozin, N. Shevchenko, M. Vinnichenko, M. Seidel, A. Kolitsch and W. Moller, *Appl. Phys. Lett.*, 2006, **89**, 061908.

31 S. Tanaka, H. Goto, H. Tomori, Y. Ootuka, K. Tsukagoshi and A. Kanda, *J. Phys.: Conf. Ser.*, 2010, **232**, 012015.

32 V. Zhukova, A. F. Cobeño, A. Zhukov, J. M. Blanco, S. Puerta, J. Gonzalez and M. Vázquez, *J. Non-Cryst. Solids*, 2001, **287**, 31–36.

33 S. G. Choi, T.-J. Ha, B.-G. Yu, S. Shin, H. H. Cho and H.-H. Park, *Thin Solid Films*, 2007, **516**, 212–215.

34 D. J. Kim, D. S. Kim, S. Cho, S. W. Kim, S. H. Lee and J. C. Kim, *Int. J. Thermophys.*, 2004, **25**, 281–289.

35 H. P. R. Frederikse, *J. Appl. Phys.*, 1961, **32**, 2211–2215.

36 D. Mardare and G. I. Rusu, *Mater. Sci. Eng., B*, 2000, **75**, 68–71.

37 J. M. Macak, K. Sirotna and P. Schmuki, *Electrochim. Acta*, 2005, **50**, 3679–3684.

38 J. M. Macák, H. Tsuchiya and P. Schmuki, *Angew. Chem., Int. Ed.*, 2005, **44**, 2100–2102.

39 C. Ruan, M. Paulose, O. K. Varghese, G. K. Mor and C. A. Grimes, *J. Phys. Chem. B*, 2005, **109**, 15754–15759.

40 J. Pan, G. Liu, G. Q. Lu and H.-M. Cheng, *Angew. Chem., Int. Ed.*, 2011, **50**, 2133–2137.

41 N. Wu, J. Wang, D. N. Tafen, H. Wang, J.-G. Zheng, J. P. Lewis, X. Liu, S. S. Leonard and A. Manivannan, *J. Am. Chem. Soc.*, 2010, **132**, 6679–6685.

42 L. Tao, Y. Xiong, H. Liu and W. Shen, *J. Mater. Chem.*, 2012, **22**, 7863–7870.

43 W. Li, C. Ni, H. Lin, C. P. Huang and S. I. Shah, *J. Appl. Phys.*, 2004, **96**, 6663–6668.

44 Q. Huang and L. Gao, *Chem. Lett.*, 2003, **32**, 638–639.

45 W. G. Bessler, *Solid State Ionics*, 2005, **176**, 997–1011.

46 T. Taguchi, Y. Saito, K. Sarukawa, T. Ohno and M. Matsumura, *New J. Chem.*, 2003, **27**, 1304–1306.

47 O. K. Varghese, D. Gong, M. Paulose, K. G. Ong, E. C. Dickey and C. A. Grimes, *Adv. Mater.*, 2003, **15**, 624–627.

48 H. Liu, L. Tao and W. Shen, *Nanotechnology*, 2011, **22**, 155603.

49 C.-Y. Chang and F.-Y. Tsai, *J. Mater. Chem.*, 2011, **21**, 5710–5715.

50 C. A. Grimes, *J. Mater. Chem.*, 2007, **17**, 1451–1457.

51 H.-T. Fang, M. Liu, D.-W. Wang, T. Sun, D.-S. Guan, F. Li, J. Zhou, T.-K. Sham and H.-M. Cheng, *Nanotechnology*, 2009, **20**, 225701.

52 J. Guo, R. J. Padilla, W. Ambrose, I. J. De Kok and L. F. Cooper, *Biomaterials*, 2007, **28**, 5418–5425.

53 L. R. Hilbert, D. Bagge-Ravn, J. Kold and L. Gram, *Int. Biodeterior. Biodegrad.*, 2003, **52**, 175–185.

54 F. Gonella, A. Quaranta, S. Padovani, C. Sada, F. D'Acapito, C. Maurizio, G. Battaglin and E. Cattaruzza, *Appl. Phys. A: Mater. Sci. Process.*, 2005, **81**, 1065–1071.

This journal is © The Royal Society of Chemistry 2013

J. Mater. Chem. A, 2013, **1**, 783–791 | **791**